Ocean Engineering 264 (2022) 112385

Contents lists available at ScienceDirect

Ocean Engineering

journal homepage: www.elsevier.com/locate/oceaneng

# Non-switching reference trajectory based discrete-time sliding mode path following control for dynamic positioning ship with time-varying disturbances

Mingyu Fu, Guorong Zhang *, Yujie Xu

*College of Intelligent Systems Science and Engineering, Harbin Engineering University, Harbin 150001, China*

ARTICLE INFO

*Keywords:*
Path following
Dynamic positioning ship
Discrete-time sliding mode control
Discrete-time disturbance observer
Discrete-time integral sliding mode surface
Reference trajectory

ABSTRACT

This paper investigates the discrete-time sliding mode (DSM) path following control problem for dynamic positioning ship (DPS) with time-varying disturbances and sideslip based on non-switching reference trajectory and discrete-time disturbance observer (DDO). Initially, a high-order DDO and a finite-time sideslip angle observer are designed to observe the time-varying disturbance and sideslip angle, respectively, to compensate for their effects on DPS. Then, the discrete-time integral sliding mode surface is designed by introducing the nonlinear integral with characteristics of small error amplification and large error saturation, which avoids the system instability due to integral saturation. Furthermore, a new DSM path following controller is designed based on the new reaching law composed of disturbance observation errors and non-switching reference trajectory. The conclusion that the position tracking error can asymptotically converge to zero is inferred. The proposed control scheme avoids the problem that the continuous-time control law is not suitable for the actual shipborne discrete-time controller and the system chattering caused by switching functions and simultaneously ensures the system's anti-disturbance ability. Finally, comparative simulation results verify the effectiveness and superiority of the proposed control scheme.

## 1. Introduction

Dynamic positioning ship (DPS) is defined by the International Maritime Organization (IMO) and classification societies of many countries, such as LR, DNV, ABS, etc., which uses active thrusters to keep its position and yaw angle on a fixed target or predetermined trajectory (Sørensen, 2011; Fu et al., 2019; Fossen, 2011). DPS has the advantages of good maneuverability, rapid movement and positioning is not affected by water depth, which plays a vital role in the field of ocean development. With the increasing demand for marine natural resources, dynamic positioning technology has been widely used in various marine applications, such as offshore oil and gas development, cable laying, dredgers, and so on (Abdelaal et al., 2018; Li et al., 2018b,a; Jung and Yoo, 2019; Islam et al., 2021).

At present, many research results are using different kinds of control methods in the research of ship's path following control (Qu et al., 2021; Gao and Guo, 2020; Zhang and Zhang, 2014). Unfortunately, the vast majority of these works are aimed at continuous-time systems. However, most modern ships, including DPS, are controlled by digital computers, and their controllers are in the form of discrete-time. They can only change the command of their actuators at the sampling instant, and the command cannot respond to the designed continuous-time controller. When the continuous-time control law is applied to the discrete-time system, the continuous-time stable system may produce complex dynamic behavior and instability due to the different stability theories. Moreover, the discrete-time system will produce some phenomena such as time delay, chattering and control command holding during the sampling time (Shao, 2015; Piorno et al., 2009; Li et al., 2020; Sheng et al., 2020). These are why it is preferable to design the control law in discrete-time for ships in practical engineering.

In the research of discrete-time control theory, sliding mode control has been widely studied in recent years because of its rapidity and strong robustness (Rubagotti et al., 2021; Sharma et al., 2021; Kang et al., 2021). Gao et al. (1995) developed the definition of quasi-sliding-mode motion and the discrete-time sliding mode (DSM) reaching law in the early days, which became a classic of DSM control theory. Later generations made a series of improvements on its basis. Ma et al. (2021) adds a high-order disturbance compensator to the reaching law to achieve accurate disturbance suppression and improve the anti-disturbance ability of the discrete-time system. Bartoszewicz and Adamiak (2020) proposes a new sliding mode control strategy based on

* Corresponding author.
*E-mail address:* guorong@hrbeu.edu.cn (G. Zhang).

https://doi.org/10.1016/j.oceaneng.2022.112385
Received 4 April 2022; Received in revised form 19 July 2022; Accepted 21 August 2022
Available online 18 September 2022

reference trajectory and adopts an external trajectory generator based on switching reaching law, which improves the anti-disturbance ability and control accuracy of the discrete-time system. On this basis, Liu et al. (2021) adds a high-order disturbance estimator, together with the reference trajectory generator, to improve the control accuracy further. However, these DSM control strategies inevitably produce chattering because the reaching law contains switching functions. For the path following control of DPS, there are also has high requirements for accuracy and reliability, and the large chattering of the control system may cause damage to the onboard actuator, and may even lead to system instability (Bessa et al., 2010). Therefore, it has become a research direction to study the DSM controller, which can not only ensure the anti-disturbance ability but also weaken chattering as much as possible. Bartoszewicz and Lesniewski (2016) improves the reaching law of Gao et al. (1995) by removing the switching function in the reaching law and introduces a new definition of DSM motion. It does not require the sliding variable to travel back and forth on the sliding mode surface (SMS) in each sampling period, greatly solving the chattering problem. However, this method of directly removing switching class functions will inevitably reduce the robustness of sliding mode control. Adamiak (2020) proposes a non-switching variable reaching law based on reference trajectory to weaken chattering and introduces a disturbance compensation method to accurate the quasi-sliding mode bandwidth to $O(T^2)$ level, and achieves good results. Regarding disturbance compensation, it is more common to design disturbance observers. In addition to the high-order disturbance estimator mentioned above, there are also commonly used discrete-time disturbance observers (DDOs) such as one-step delay disturbance observer (Xu, 2016), proportional–integral observer (PIO) (Chang, 2006), and so on. However, most of them make the bandwidth of the sliding variable depend on the step size of the sampling time, which cannot meet the requirements in some applications. In this paper, by improving the high-order disturbance observer in Fu and Li (2022), the bandwidth of the sliding variable is only related to the order of the observer itself, and the observation accuracy can tend to zero with the increase of the order.

In addition, compared with the diversity of the design of SMS in continuous-time sliding mode control, such as adaptive integral SMS (Gonzalez-Garcia and Castaeda, 2021; Shao et al., 2021), LQR-SMS (Sanjeewa and Parnichkun, 2021; Mathiyalagan and Sangeetha, 2020), fast iterative terminal SMS (Hu et al., 2021; Van et al., 2019) and so on, the number and variety of SMS design of DSM are less. Most of the DSM control works reviewed above use the simplest proportional–integral SMS, which restricts the robustness of the control system to a certain extent. Therefore, when studying the reaching law to weaken the chattering of DSM control and ensure the system's robustness, it is also necessary to consider the design and research of discrete-time SMS.

Motivated by the above considerations, a DSM path following control scheme based on the non-switching reference trajectory and DDO is designed. It solves the DPS's path following control problem with time-varying environmental disturbances, sideslip, and DSM chattering. The main features and contributions of this paper are summarized as follows:

(1) A new DSM path following control scheme based on the non-switching reference trajectory is proposed to avoid the problem that continuous-time control laws are unsuitable for actual shipborne discrete-time controllers. While ensuring the anti-disturbance ability of the system, the chattering caused by switching functions in the traditional DSM control is weakened.

(2) The high-order DDO of Fu and Li (2022) is improved to expand its scope of application, and the disturbance terms in the reaching law of Bartoszewicz and Lesniewski (2016) and Adamiak (2020) are replaced by the disturbance observation error. The chattering caused by inaccurate disturbance assumptions is eliminated, and the sliding variable bandwidth no longer depends on the sampling time but only on the observer's order.

(3) A new discrete-time nonlinear integral SMS is designed by introducing a saturation function with small error amplification and large error saturation characteristics. The problem of system instability due to integral saturation is solved, and the robustness is enhanced.

The rest of this paper is organized as follows. The preliminaries and problem formulation are introduced in Section 2. In Section 3, the design of guidance law based on sideslip angle observation is introduced. The design of the DSM controller is introduced in Section 4. The stability of the control system is analyzed in Section 5. Comparative simulation results are given and analyzed in Section 6. Conclusions are given in Section 7.

## 2. Preliminaries and problem formulation

### 2.1. Preliminaries

**Definition 1** (*Bartoszewicz, 1998*)**.** We call the quasi-sliding mode in the $\delta$ vicinity of the sliding hyperplane $s(k) = 0$ such a motion of the system that

$$|s(k)| \leqslant \delta \tag{1}$$

where the positive constant $\delta$ is called the quasi-sliding-mode bandwidth.

**Definition 2** (*Bartoszewicz, 1998*)**.** We say that the control system satisfies the reaching condition of the quasi-sliding mode in the $\delta$ vicinity of the sliding surface $s(k) = 0$ if for any $k \geqslant 0$, the following conditions are satisfied:

$$\begin{aligned} &s(k) > \delta \Rightarrow -\delta \leqslant s(k+1) < s(k) \\ &s(k) < -\delta \Rightarrow s(k) \leqslant s(k+1) < \delta \\ &|s(k)| \leqslant \delta \Rightarrow |s(k+1)| \leqslant \delta \end{aligned} \tag{2}$$

where $\delta$ is a positive constant.

**Lemma 1** (*Shtessel et al., 2007*)**.** *Consider SISO dynamics $\dot{\chi} = \rho(t)+u, \chi \in \mathbb{R}$. Let the variable $\rho(t)$ be $q-1$ times differentiable so that $\rho^{q-1}(t)$ has a Lipschitz constant $L > 0$.*

Then, consider the following observer:

$$\begin{cases} \dot{z}_0 = \gamma_0 + u, \\ \gamma_0 = -\lambda_0 L^{1/(q+1)} |z_0 - \chi|^{q/(q+1)} \mathrm{sign}(z_0 - \chi) + z_1, \\ \dot{z}_1 = \gamma_1, \\ \gamma_1 = -\lambda_1 L^{1/q} |z_1 - \gamma_0|^{(q-1)/q} \mathrm{sign}(z_1 - \gamma_0) + z_2, \\ \vdots \\ \dot{z}_{q-1} = \gamma_{q-1}, \\ \gamma_{q-1} = -\lambda_{q-1} L^{1/2} |z_{q-1} - \gamma_{q-2}|^{1/2} \mathrm{sign}(z_{q-1} - \gamma_{q-2}) + z_q, \\ \dot{z}_q = -\lambda_q L \mathrm{sign}(z_q - \gamma_{q-1}). \end{cases} \tag{3}$$

Suppose that $\chi(t)$ and $u(t)$ are measured with some Lebesgue-measurable noises bounded, respectively, by $\varepsilon > 0$ and $\varsigma\varepsilon^{(q-1)/q}, \varsigma > 0$, is any fixed constant. The parameters $\lambda_i$ being chosen sufficiently large in the reverse order, the following inequalities are established in finite time for some positive constants $\mu_i, \eta_i$ depending exclusively on $\varsigma$ and the choice of parameters:

$$\begin{cases} |z_0 - \chi(t)| \leqslant \mu_0 \varepsilon \\ \vdots \\ |z_i - \rho^{(i-1)}(t)| \leqslant \mu_i \varepsilon^{(q-i+1)/(q+1)}, i = 1, \ldots, q, \\ |\gamma_j - \rho^{(j)}(t)| \leqslant \eta_j \varepsilon^{(q-j)/(q+1)}, j = 1, \ldots, q-1. \end{cases} \tag{4}$$

### 2.2. Modeling of DPS

According to Skjetne et al. (2004), the continuous-time mathematical model of the DPS can be represented as follows:

$$\dot{\eta} = R(\psi)\nu \tag{5}$$

$$M\dot{\nu} + C(\nu)\nu + D(\nu)\nu = \tau + \omega \tag{6}$$

where $\eta = [x, y, \psi]^T$ represents the position and heading angle of the DPS in the earth-fixed inertial frame; $\nu = [u, v, r]^T$ represents the vector of surge velocity, sway velocity and yaw rate of the ship in the body-fixed frame; $R(\psi)$ is the transformation matrix from the body-fixed frame to the earth-fixed inertial frame; $M$, $C(\nu)$ and $D(\nu)$ are inertia matrix, Coriolis centripetal force matrix and damping coefficient matrix, respectively; $\tau = [\tau_u, \tau_v, \tau_r]^T$ represents the control input vector; $\omega = [\omega_u, \omega_v, \omega_r]^T$ represents the forces and moment generated by time-varying environmental disturbances. Among them, the specific expressions of $M$, $D(\nu)$, $R(\psi)$ and $C(\nu)$ are as follows:

$$M = \begin{bmatrix} m - X_{\dot{u}} & 0 & 0 \\ 0 & m - Y_{\dot{v}} & mx_g - Y_{\dot{r}} \\ 0 & mx_g - N_{\dot{v}} & I_z - N_{\dot{r}} \end{bmatrix} \tag{7}$$

$$D(\nu) = \begin{bmatrix} X_u & 0 & 0 \\ 0 & Y_v & Y_r \\ 0 & N_v & N_r \end{bmatrix}, \; R(\psi) = \begin{bmatrix} \cos\psi & -\sin\psi & 0 \\ \sin\psi & \cos\psi & 0 \\ 0 & 0 & 1 \end{bmatrix} \tag{8}$$

$$C(\nu) = \begin{bmatrix} 0 & 0 & -(m - Y_{\dot{v}})v \\ 0 & 0 & (m - X_{\dot{u}})u \\ (m - Y_{\dot{v}})v & -(m - X_{\dot{u}})u & 0 \end{bmatrix} \tag{9}$$

where $m$ is the mass of the DPS; $X_{\dot{u}}$, $Y_{\dot{v}}$, $N_{\dot{r}}$, $Y_{\dot{r}}$ and $N_{\dot{v}}$ are additional masses generated by hydrodynamic forces; $x_g$ is the surge distance from the origin to the center of gravity; $X_u$, $Y_v$, $Y_r$, $N_v$ and $N_r$ are linear damping coefficients of the ship's hydrodynamic forces.

In order to retain the structural form of the original continuous nonlinear model and facilitate the design of the controller, the first-order Euler approximate forward difference method is adopted. The derivative term in the model is replaced by the difference quotient of the function value on the grid node. Then the mathematical models (5) and (6) can be rewritten as follows:

$$\frac{\eta(k+1) - \eta(k)}{h} = R(\psi(k))\nu(k) \tag{10}$$

$$M\frac{\nu(k+1) - \nu(k)}{h} + C(\nu(k))\nu(k) + D(\nu(k))\nu(k) = \tau(k) + \omega(k) \tag{11}$$

The discretized models of the DPS can be reorganized as follows:

$$\eta(k+1) = \eta(k) + hR(k)\nu(k) \tag{12}$$

$$\nu(k+1) = \nu(k) + hM^{-1}[\tau(k) + \omega(k) - C(k)\nu(k) - D(k)\nu(k)] \tag{13}$$

To simplify the writing of the formula, denote the matrices $C(\nu(k))$, $D(\nu(k))$ and $R(\psi(k))$ as $C(k)$, $D(k)$ and $R(k)$.

(13) can be further written in the following form:

$$\nu(k+1) = \Phi(k)\nu(k) + \Gamma\tau(k) + d(k) \tag{14}$$

where $\Phi(k) = hM^{-1}[M/h - C(k) - D(k)]$, $\Gamma = hM^{-1}$, $d(k) = hM^{-1}\omega(k)$ and $h$ is the sampling period.

### 2.3. Control objective

In this paper, we consider designing a DSM control scheme to realize the fast and accurate path following of a DPS with external environmental disturbances and time-varying sideslip. Under the designed control law, the distance error of following the desired path can converge to zero.

This paper considers the indirect control scheme, the distance tracking error control is transformed into the velocity tracking error control. Furthermore, a controller is designed to control the velocity of the DPS, and the indirect control of the distance tracking error is realized.

As shown in Fig. 1, the line-of-sight (LOS) method defines the distance between the DPS and the target tracking point. The distance error of DPS path following is defined as follows:

$$\begin{aligned} \Theta(k) &= \sqrt{[x(k) - x_d(k)]^2 + [y(k) - y_d(k)]^2} \\ &= \sqrt{x_e^2(k) + y_e^2(k)} \end{aligned} \tag{15}$$

The control objective is to make the distance error $\Theta(k)$ satisfy:

$$\Theta(k) \to 0\,, \; k \to \infty \tag{16}$$

Before the path following controller design, we make the assumptions as follows.

**Assumption 1.** The disturbance $d_j(k), j = u, v, r$ are bounded, and the change rate of $d_j(k)$ at any $k$ instant satisfies $|\Delta d_j(k)| < 1$, i.e., $|\Delta\omega_i(k)| < (MI_{3\times1})_i/h, i = 1, 2, 3$, where $I_{3\times1}$ is a vector with dimension $3 \times 1$ whose elements are all one.

**Assumption 2.** The desired path $\eta_d = [x_d(\theta), y_d(\theta), \psi_d(\theta)]^T$ is a smooth curve with $\theta$ as the dynamic parameter on the horizontal plane to be designed, and $\eta_d$, $\dot{\eta}_d$ and $\ddot{\eta}_d$ exist and are bounded.

**Remark 1.** In practical engineering, the external environmental disturbance is caused by wind, waves and ocean currents, and its change rate is bounded. Under normal circumstances, external environmental disturbances change slowly, and the change rate will increase sharply only in extreme cases. Assumption 1 in this paper requires that the variation of the environmental disturbance force in each sampling period is less than the magnitude of the inertial matrix of the ship. While the sampling period is usually small, and the order of magnitude of the inertia matrix is large, Assumption 1 is reasonable.

## 3. Design of guidance law

LOS guidance law is a guidance method widely used in ship path following. To overcome the guiding problem of ship with sideslip angle, some guidance laws such as integral LOS (ILOS), adaptive LOS (ALOS), extended state observer (ESO)-based LOS have been proposed (Wu et al., 2022; Liu et al., 2017; Peng and Wang, 2018). However, none of them take into account the time required to compensate for the effects of the sideslip angle. In this section, a LOS guidance law based on a finite-time sideslip angle observer (FTSAO) is designed to realize the compensation of the sideslip angle in a finite time.

### 3.1. Establishment of position error system

As shown in Fig. 1, the point $P_P(\theta) = [x(\theta), y(\theta)]^T$ on the continuous smooth desired path is the current target tracking point and satisfies $x^2(\theta) + y^2(\theta) \neq 0$, and the $SF$ coordinate system is constructed with $P_P(\theta)$ as the origin. Define $\psi(\theta)$ as the rotation angle from the North-East coordinate system to the $SF$ coordinate system, then $\psi(\theta) = \arctan 2(y'(\theta), x'(\theta))$. To facilitate the following description, make the following brief notes: $x_\theta \triangleq x(\theta)$, $y_\theta \triangleq y(\theta)$, $\psi_\theta \triangleq \psi(\theta)$, $(.)'(\theta) \triangleq d(.)/d\theta$.

Define the position and heading error vector under the $SF$ coordinate system as $\eta_e^S = [x_e, y_e, \psi_e]^T$, and the position and heading error vector under the North-East coordinate system as $\eta_e^N = [x - x_\theta, y - y_\theta, \psi - \psi_\theta]^T$. From the properties of the diffeomorphic transformation, it can be known that the convergence of $\eta_e^S$ in the $SF$ coordinate system is equivalent to the convergence of $\eta_e^N$ in the North-East coordinate system (Wang, 2019). Therefore, the convergence of $\eta_e^N$ in the North-East coordinate system can be achieved by indirectly designing the controller to ensure the convergence of $\eta_e^S$ in the $SF$ coordinate system.

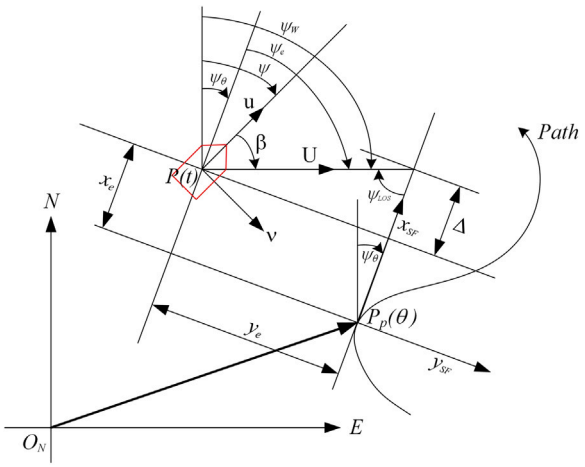


**Fig. 1.** The guidance schematic diagram.

The derivatives of $x_e$, $y_e$ and $\psi_e$ of the DPS in the $SF$ coordinate system can be derived as follows (Wang, 2019):

$$\begin{bmatrix}\dot{x}_e\\ \dot{y}_e\\ \dot{\psi}_e\end{bmatrix}=\begin{bmatrix}U\cos\left(\psi-\psi_\theta+\beta\right)+\dot{\psi}_\theta y_e-\dot{\theta}\sqrt{x_\theta'^2+y_\theta'^2}\\ U\sin\left(\psi-\psi_\theta+\beta\right)-\dot{\psi}_\theta x_e\\ r-\dot{\psi}_\theta+\dot{\beta}\end{bmatrix} \tag{17}$$

### 3.2. Design of finite-time sideslip angle observer

According to Fig. 1, the expression of the sway position error derivative in (17) can be further expanded as

$$\begin{aligned}\dot{y}_e&=U\sin\left(\psi-\psi_\theta+\beta\right)-\dot{\psi}_\theta x_e\\&=u\sin\left(\psi-\psi_\theta\right)+u\cos\left(\psi-\psi_\theta\right)\tan\beta-\dot{\psi}_\theta x_e\\&=Y\left(u,\psi,\psi_\theta,\beta\right)+u\sin\left(\psi-\psi_\theta\right)-\dot{\psi}_\theta x_e\end{aligned} \tag{18}$$

where $Y\left(u,\psi,\psi_\theta,\beta\right)=u\cos\left(\psi-\psi_\theta\right)\tan\beta$ is continuously differentiable and $\beta=\arctan 2\left(v,u\right)$ represents the sideslip angle of the DPS.

The designed FTSAO is as follows (Wang and Ki Ahn, 2020):

$$\begin{cases}\hat{\dot{y}}_e=\Lambda+u\sin\left(\psi-\psi_\theta\right)-\dot{\psi}_\theta x_e\\ \Lambda=-\varphi_1 W^{1/2}\left|\hat{y}_e-y_e\right|^{1/2}\mathrm{sign}\left(\hat{y}_e-y_e\right)+\hat{Y}\\ \hat{\dot{Y}}=-\varphi_2 W\,\mathrm{sign}\left(\hat{Y}-\Lambda\right)\\ \hat{\beta}=\arctan\{\hat{Y}/[u\cos(\psi-\psi_\theta)]\}\end{cases} \tag{19}$$

where $\varphi_i>0(i=1,2)$, $W>0$ and $\hat{Y}(0)=0$.

**Theorem 1.** *The sideslip angle observer designed according to (19) can realize that the time-varying sideslip angle observation error of the DPS converges to zero in a finite time.*

**Proof.** Derivating $Y$ to get:

$$\begin{aligned}\dot{Y}&=\dot{v}\cos(\psi-\psi_\theta)-v\sin(\psi-\psi_\theta)(\dot{\psi}-\dot{\psi}_\theta)\\&=\dot{v}\cos(\psi-\psi_\theta)-v\sin(\psi-\psi_\theta)(r-\dot{\psi}_\theta)\end{aligned} \tag{20}$$

Considering the practical engineering application of the DPS, the actuator input will be saturated, and the actual velocity and the change rate of the sway velocity are bounded, i.e., $u$, $v$, $r$ and $\dot{v}$ are bounded. $\dot{\psi}_\theta$ is determined by the preset desired path, which is also bounded. Therefore, $\dot{Y}$ is bounded, i.e., $|\dot{Y}|\le G<\infty$ for a constant $G>0$.

Define the observation errors as

$$e_1=\hat{y}_e-y_e\ ,\quad e_2=\hat{Y}-Y \tag{21}$$

Derivating the observation errors of (21) to $y_e$ and $Y$, we get:

$$\begin{aligned}\dot{e}_1&=\hat{\dot{y}}_e-\dot{y}_e\\&=-\varphi_1 W^{1/2}\left|\hat{y}_e-y_e\right|^{1/2}\mathrm{sign}\left(\hat{y}_e-y_e\right)+Y+u\sin\left(\psi-\psi_\theta\right)-\dot{\psi}_\theta x_e-\dot{y}_e\\&=-\varphi_1 W^{1/2}\left|\hat{y}_e-y_e\right|^{1/2}\mathrm{sign}\left(\hat{y}_e-y_e\right)+\hat{Y}-Y\\&=-\varphi_1 W^{1/2}\left|e_1\right|^{1/2}\mathrm{sign}\left(e_1\right)+e_2\end{aligned} \tag{22}$$

$$\begin{aligned}\dot{e}_2&=\hat{\dot{Y}}-\dot{Y}\\&\in-\varphi_2 W\,\mathrm{sign}\left(e_2-\dot{e}_1\right)+[-G,G]\end{aligned} \tag{23}$$

In Lemma 1, taking $\chi(t)=0$ and $u(t)=0$, it can be concluded that system

$$\begin{cases}\dot{z}_1=-\lambda_1 L^{1/2}|z_1|^{1/2}\mathrm{sign}(z_1)+z_2\\ \dot{z}_2\in-\lambda_2 L\mathrm{sign}(z_2-\dot{z}_1)+[-L,L]\end{cases} \tag{24}$$

has a time constant $t_{ob}$, and for any time $t\ge t_{ob}$, there are $z_i(t)=0, i=1,2$. Where $\lambda_i>0(i=1,2)$ and $L>0$.

Then according to this conclusion, taking $W=\max\{W,G\}$, the observation errors $e_1$ and $e_2$ will converge to zero in a finite time. That is, $\exists\ t_{ob}>0$, for $\forall\ t\ge t_{ob}$, we have

$$\hat{y}_e(t)\equiv y_e(t)\quad,\quad\hat{Y}(t)\equiv Y(t) \tag{25}$$

Therefore, when the observation value $\hat{Y}$ of $Y$ is known, $\hat{\beta}$ is known, and the sideslip angle observation error will converge to zero within a finite time.

### 3.3. Design of FTSAO-based guidance law

Referring to the existing literature on LOS guidance algorithm (Fu et al., 2022), the FTSAO-based LOS guidance law can be designed as follows

$$\begin{cases}\dot{\theta}=[k_x x_e+U\cos(\psi-\psi_\theta+\hat{\beta})]/\sqrt{x_\theta'^2+y_\theta'^2}\\ \psi_d=\psi_\theta+\arctan(-y_e/\Delta-\tan\hat{\beta})\\ \hat{\beta}=\arctan\{\hat{Y}/[u\cos(\psi-\psi_\theta)]\}\end{cases} \tag{26}$$

where $\Delta>0$ is the forward-looking distance parameter.

Let $\theta$ be updated according to (26), and design the controller so that the heading $\psi$ of the DPS tracks $\psi_d$ of (26). If the tracking error can converge to zero asymptotically, then using this guidance system can ensure that $(x_e,y_e)$ can converge to zero asymptotically so that the DPS follows the desired path. The specific proof process can be found in Fu et al. (2022).

In order to make the forward-looking distance parameter $\Delta$ better cope with the navigation state change of the DPS, the following adaptive forward-looking distance parameter is designed:

$$\Delta=\left(\Delta_{\max}-\Delta_{\min}\right)e^{-\kappa y_e^2}+\Delta_{\min} \tag{27}$$

where $\kappa$ is a non-negative parameter.

It can be seen from (27) that when $y_e$ is larger, $\Delta$ approaches $\Delta_{\min}$, making $y_e$ of the DPS converge faster; when $y_e$ is smaller, $\Delta$ approaches $\Delta_{\max}$, which helps avoid $y_e$ overshooting near the desired path. By setting different constant values of $\Delta$ for many experiments, the appropriate critical values for $\Delta_{\min}$ and $\Delta_{\max}$ can be found. The parameter $\kappa$ is used to adjust the response speed of the adaptive parameter $\Delta$ to the change of $y_e$, and the larger the parameter $\kappa$, the faster the response of $\Delta$. The parameter $k_x$ is used to adjust the convergence speed of $x_e$. The larger $k_x$, the faster $x_e$ converges. The design of parameters $\varphi_i, i=1,2$ and $W$ of FTSAO can be found in Shtessel et al. (2007).

## 4. Design of path following control algorithm

### 4.1. Design of virtual heading controller

The Lyapunov function is constructed as follows:

$$V_\psi(k)=\psi_e^2(k)/h \tag{28}$$

Based on (28), the first-order difference of the Lyapunov function can be derived as

$$\begin{aligned}\Delta V_\psi(k) &= V_\psi(k+1) - V_\psi(k)\\ &= [\psi_e^2(k+1) - \psi_e^2(k)]/h\\ &= [\psi_e(k+1) - \psi_e(k) + 2\psi_e(k)][\psi_e(k+1) - \psi_e(k)]/h\\ &= [\psi_e(k+1) - \psi_e(k)]^2/h + 2\psi_e(k)[\psi_e(k+1) - \psi_e(k)]/h\\ &= \left[\psi(k+1) - \psi(k) - \psi_d(k+1) + \psi_d(k)\right]^2/h\\ &\quad + 2\psi_e(k)\left[\psi(k+1) - \psi(k) - \psi_d(k+1) + \psi_d(k)\right]/h\end{aligned} \tag{29}$$

To stabilize $V_\psi$, a virtual control law is designed as follows:

$$r_d(k+1) = [\psi_d(k+1) - \psi_d(k)]/h - \xi\psi_e(k) \tag{30}$$

Then

$$\begin{aligned}\Delta V_\psi(k) &= h\xi^2\psi_e^2(k) - 2\xi\psi_e^2(k)\\ &= (h\xi^2 - 2\xi)\psi_e^2(k)\end{aligned} \tag{31}$$

where $\xi$ is a positive parameter. Selecting the parameter $\xi \in (0, \frac{2}{h})$, then $h\xi^2 - 2\xi < 0$.

If and only if $\psi_e(k) = 0$, there is $\Delta V_\psi(k) = 0$. Therefore, when the virtual heading controller $r_d(k)$ is designed according to (30), the tracking error of the DPS to the desired heading can converge to zero asymptotically.

### 4.2. Design of high-order DDO

For the DPS with measurable output and unknown disturbances in this paper, a high-order DDO is designed to observe external environmental disturbances effectively. The high-order DDO is designed as follows:

$$\begin{cases}\hat{v}(k) = Av(k-1) + B\tau(k-1) + \hat{d}(k-1)\\ \hat{d}(k) = \hat{d}(k-1) + L_0[v(k) - \hat{v}(k)] + \Delta\hat{d}(k-1) + L_1[\Delta v(k) - \Delta\hat{v}(k)]\\ \qquad + \cdots + \Delta^N\hat{d}(k-1) + L_N[\Delta^N v(k) - \Delta^N\hat{v}(k)]\end{cases} \tag{32}$$

where $A = hM^{-1}[-C(v) - D(v) + h^{-1}M]$, $B = hM^{-1}$, and the positive integer $N$ is the order of the high-order DDO. $\hat{d}(k)$ and $\hat{v}(k)$ are the disturbance observation value and output observation value of the system at instant $k$, respectively. $\Delta = 1 - z^{-1}$ is a first-order difference operator and $z^{-1}$ is a unit-backward operator. $\Delta\hat{d}(k-1) = \hat{d}(k-1) - \hat{d}(k-2)$ is the difference of disturbance observation values between instants $k-1$ and $k-2$. $\Delta v(k) = v(k) - v(k-1)$ is the difference of system output between instants $k$ and $k-1$. $\Delta\hat{v}(k) = \hat{v}(k) - \hat{v}(k-1)$ is the difference of system output observation values between instants $k$ and $k-1$. $L_i \in \mathbb{R}, i = 0, 1, 2, \ldots, N$ are constants.

**Theorem 2.** *If Assumption 1 holds, and there are constants $L_i \in \mathbb{R}, i = 0, 1, 2, \ldots, N$ such that for any $|z| > 1$, the inequality*

$$[1 - G(z^{-1})z^{-1} + Q(z^{-1})z^{-1}] \neq 0 \tag{33}$$

*holds, then for any positive integer $N$, the absolute values $|\tilde{d}_j(k)|, j = u, v, r$ of the observation error are always bounded. And for any small positive number $\varepsilon > 0$, there is a positive integer $N_0$, when $N > N_0$, the disturbance observation error satisfies*

$$|d_j(k) - \hat{d}_j(k)| < \varepsilon, j = u, v, r \tag{34}$$

*that is,*

$$\lim_{N\to\infty} |d_j(k) - \hat{d}_j(k)| = 0 \tag{35}$$

*where*

$$G(z^{-1}) = 1 + \Delta + \Delta^2 + \cdots + \Delta^N, \tag{36}$$

$$Q(z^{-1}) = L_0 + L_1\Delta + \cdots + L_N\Delta^N. \tag{37}$$

**Proof.** For any disturbance $d(k+1)$, it can be extended to the following form:

$$d(k+1) = d(k) + \Delta d(k) + \Delta^2 d(k) + \cdots + \Delta^N d(k) + \Delta^{N+1} d(k+1) \tag{38}$$

Define the disturbance observation error and the output observation error as

$$\tilde{d}(k) = d(k) - \hat{d}(k) \tag{39}$$

$$\tilde{v}(k) = v(k) - \hat{v}(k) \tag{40}$$

From (14) and (32), we can get

$$\tilde{v}(k) = \tilde{d}(k-1) \tag{41}$$

Subtracting (32) from (38) and substituting (36), (37) and (40) in, we get

$$\begin{aligned}&\tilde{d}(k+1) = d(k+1) - \hat{d}(k+1)\\ &= (1 + \Delta + \Delta^2 + \cdots + \Delta^N)\tilde{d}(k)\\ &\quad - (L_0 + L_1\Delta + L_2\Delta^2 + \cdots L_N\Delta^N)\tilde{v}(k+1) + \Delta^{N+1}d(k+1)\\ &= G(z^{-1})\tilde{d}(k) - Q(z^{-1})\tilde{v}(k+1) + \Delta^{N+1}d(k+1)\end{aligned} \tag{42}$$

Substituting (41) into (42) to get

$$[1 - G(z^{-1})z^{-1} + Q(z^{-1})z^{-1}]\tilde{d}(k) = \Delta^{N+1}d(k) \tag{43}$$

From Assumption 1, we know that for any small positive number $\varepsilon > 0$, there exists a positive integer $N_0$, when $N > N_0$, $|\Delta^{N+1}d_j(k)| < \varepsilon$ holds, i.e., $\lim_{N\to\infty} d_j(k) = 0$ where $j = u, v, r$. Then from (33), it can be seen that the disturbance observation error $\tilde{d}(k)$ satisfies

$$\lim_{N\to\infty} \tilde{d}_j(k) = 0, j = u, v, r \tag{44}$$

From (43), we get:

$$\tilde{d}(k) = \frac{\Delta^{N+1}d(k)}{1 - G(z^{-1})z^{-1} + Q(z^{-1})z^{-1}} \tag{45}$$

From Assumption 1, we can also know that for any positive integer $N$, there is $|\Delta^{N+1}d_j(k)| < 1$. Then we have:

$$\begin{aligned}|\tilde{d}_j(k)| &= \left|\frac{\Delta^{N+1}d_j(k)}{1 - G(z^{-1})z^{-1} + Q(z^{-1})z^{-1}}\right|\\ &< \frac{1}{|1 - G(z^{-1})z^{-1} + Q(z^{-1})z^{-1}|}\\ &\triangleq \lambda\end{aligned} \tag{46}$$

where $\lambda \geqslant 0$ is the upper bound of $|\tilde{d}_j(k)|$.

### 4.3. Design of DSM controller

In this paper, we apply the modified definition (Bartoszewicz, 1998) of the quasi-sliding mode, that is, the system's state keeps moving around a given sliding hyperplane. According to this definition, in the quasi-sliding mode, the system state trajectory is kept within the specified range around the hyperplane, but does not necessarily pass through the sliding hyperplane in each control period.

Define the velocity tracking error as

$$e(k) = v_d(k) - v(k) \tag{47}$$

Design the discrete-time integral SMS as follows:

$$\begin{cases}\sigma(k) = C_1 e(k) + b(k)\\ b(k) = b(k-1) + C_2 e(k-1)\end{cases} \tag{48}$$

where $\sigma(k) \in \mathbb{R}^3$, $b(k) \in \mathbb{R}^3$, and $b(0) = \mathbf{0}$. $C_i = diag(c_{iu}, c_{iv}, c_{ir}), i = 1, 2$ are constant matrices to be designed and satisfy $(C_1\Gamma)^{-1} \neq \mathbf{0}$ and $c_{ij} > 0, j = u, v, r$.

Due to the use of integral control, when the initial error is large, it may lead to an integral saturation effect and make the system unstable.

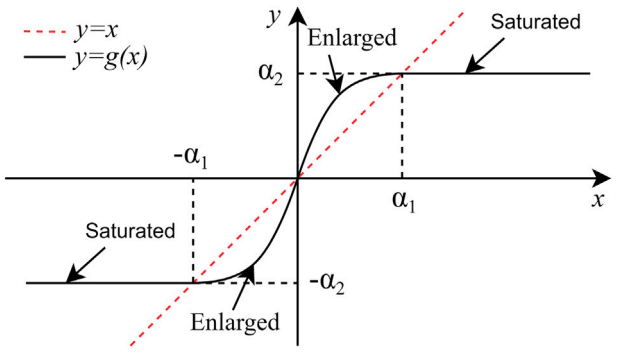


**Fig. 2.** The graph of functions $y = x$ and $y = g(x)$.

Therefore, inspired by Hu et al. (2018), Peng and Zheng (2011), a class of nonlinear saturation functions is introduced:

$$g(x) = \begin{cases} \alpha_2 \sin[\pi x/(2\alpha_1)], & |x| \leqslant \alpha_1 \\ \alpha_2 \mathrm{sign}(x), & |x| > \alpha_1 \end{cases} \tag{49}$$

where $\alpha_1$ and $\alpha_2$ are positive constants.

As shown in Fig. 2, compared with the traditional linear function, this nonlinear function has the characteristics of small error amplification and large error saturation.

Therefore, the nonlinear integral can replace the traditional integral, and the discrete-time integral SMS becomes

$$\begin{cases} \sigma(k) = C_1 e(k) + b(k) \\ b(k) = b(k-1) + C_2 \mathbf{g}[e(k-1)] \end{cases} \tag{50}$$

where $\mathbf{g}[e(k-1)] = [g[e_u(k-1)], g[e_v(k-1)], g[e_r(k-1)]]^T$.

We use $\sigma_g(k)$ to denote the reference sliding variable and generate its desired change externally. The reference trajectory is determined by the mathematical model of the DPS that removes external environmental disturbances. In order to ensure that the perturbed system converges monotonically to the sliding hyperplane, the same initial conditions are set for the two sliding variables $\sigma(k)$ and $\sigma_g(k)$. So

$$\sigma_g(0) = \sigma(0) = C_1[v_d(0) - v(0)] \tag{51}$$

The reference trajectory of the non-switching variable type is designed as

$$\sigma_g(k+1) = \left\{I - q[\sigma_g(k)]\right\} \sigma_g(k) \tag{52}$$

where $q$ is defined by the following function:

$$\left\{q[\sigma_g(k)]\right\}_{ij} = \begin{cases} \dfrac{(\sigma_0)_i}{\left|[\sigma_g(k)]_i\right| + (\sigma_0)_i} \in (0,1] \ , & i = j \\ 0 \qquad\qquad\qquad\quad , & i \neq j \end{cases} \tag{53}$$

where $(\sigma_0)_i$ are positive constants and $i, j = 1, 2, 3$.

Compared with the reference trajectory of the switching variable type of Bartoszewicz and Adamiak (2020), the reference trajectory of the non-switching variable type in this paper does not contain sign functions and saturation functions. Thus, the jump of the sliding mode variable is avoided, and the adverse effect of chattering is greatly weakened.

The DSM reaching law is designed as

$$\sigma(k+1) = \sigma_g(k+1) - C_1 \tilde{d}(k) \tag{54}$$

where $\tilde{d}(k) = d(k) - \hat{d}(k)$ is the observation error of the disturbance observer.

In the non-reference trajectory strategy represented by Bartoszewicz and Lesniewski (2016), the value of $\sigma(k+1)$ depends on $\sigma(k)$. Therefore, it is affected by all disturbance values from the beginning of the control process. In the reaching law of this paper, the sliding mode variable of the control plant is controlled according to the desired reference trajectory, independent of disturbances. $\sigma(k+1)$ is only affected by the disturbance $d(k)$ of one control step size but not by the previous disturbance values $d(0)$, $d(1)$, …, and $d(k-1)$. Therefore, the reaching law of this paper ensures the improvement of system robustness by reducing the influence of disturbance on the state.

Considering (14), (48) and (54), we can get the following control law (see Fig. 3) :

$$\begin{aligned} \tau(k) = (C_1\Gamma)^{-1}[&C_1 v_d(k+1) + b(k+1) - \sigma_g(k+1) \\ &- C_1\hat{d}(k) - C_1\Phi(k)\nu(k)] \end{aligned} \tag{55}$$

**Remark 2.** Two non-core parts of the sideslip angle observer and guidance law before the controller design in this paper are still of continuous-time type. We realize the conversion between discrete-time and continuous-time quantities by setting the holder and sampling quantization structure in these two parts. Since these two parts belong to data processing, the desired heading angle is calculated according to the position and heading of the current ship relative to the desired path, so the approximate transformation of its data type has little impact on the whole control scheme.

## 5. Stability analysis

**Theorem 3.** *For any initial value of the state variables of the DPS, the sliding mode reference variable $\sigma_g(k)$, determined by the reaching law (52), will asymptotically converge to the sliding hyperplane as the parameter $k$ increases.*

**Proof.** Consider the following Lyapunov function:

$$V(k) = \left|[\sigma_g(k)]_i\right|, i = u, v, r \tag{56}$$

The first-order difference of $V(k)$ can be derived as

$$\begin{aligned} \Delta V(k) &= V(k+1) - V(k) \\ &= \left|[\sigma_g(k+1)]_i\right| - \left|[\sigma_g(k)]_i\right| \\ &= \left|[\sigma_g(k)]_i\right| \frac{-(\sigma_0)_i}{\left|[\sigma_g(k)]_i\right| + (\sigma_0)_i} \\ &\leqslant 0 \end{aligned} \tag{57}$$

if and only if $[\sigma_g(k)]_i = 0$, there is $\Delta V(k) = 0$.

Therefore, according to the discrete-time Lyapunov stability theory, for any initial value of the sliding mode function, the sliding mode reference variable $[\sigma_g(k)]_i$ will asymptotically converge to $[\sigma_g(k)]_i$=0 with the increase of the parameter $k$.

**Theorem 4.** *The DSM closed-loop control system composed of (14), (30) and (55) is robust stable. If the selection of positive parameters $\alpha_1$ and $\alpha_2$ satisfies $\alpha_2 c_{1i}^{-1} c_{2i} < 4\alpha_1/\pi, i = u, v, r$, and the order of the high-order DDO is high enough, the position tracking error of the DPS can asymptotically converge to zero.*

**Proof.** $\sigma(k)$ can be regarded as composed of the sum $\sigma_1(k) + \sigma_2(k)$ of $\sigma_1(k)$ and $\sigma_2(k)$, then the sliding mode dynamic expression (54) can be decomposed into

$$\begin{cases} \sigma_1(k) = \sigma_g(k) \\ \sigma_2(k) = -C_1\tilde{d}(k) \end{cases} \tag{58}$$

According to Theorem 3, there must be some time $k_0$ such that $\sigma_1(k_0 + j) = \mathbf{0}, j = 0, 1, 2, \ldots$. Also known from Theorem 2, when the order of the high-order DDO is high enough, the disturbance observation error converges asymptotically and satisfies $\lim_{N\to\infty} \tilde{d}(k) = \mathbf{0}$, then $\sigma_2(k) = \mathbf{0}$. So when $k > k_0$, $\sigma(k+1) = \sigma_1(k+1) + \sigma_2(k+1) = \mathbf{0}$ must be established. Therefore, the closed-loop system's actual sliding mode dynamic function must converge and stabilize on the ideal sliding

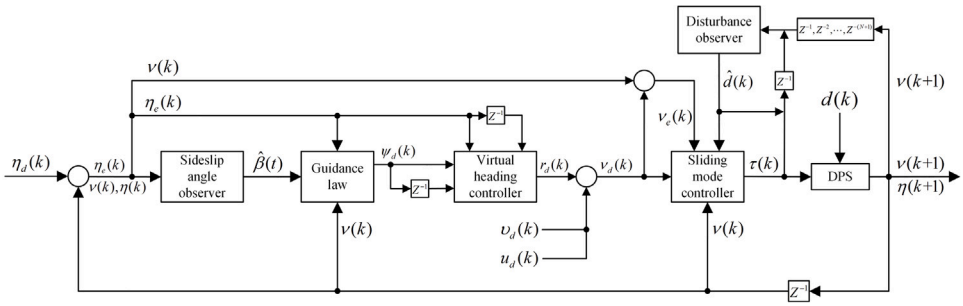


**Fig. 3.** The block diagram of control scheme.

hyperplane. Since the stability and dynamic quality of the ideal sliding hyperplane can be guaranteed by the design of pole configuration and other methods, the DSM closed-loop control system composed of (14), (30) and (55) is robust stable.

Given (14) and (47), the one-step forward error equation can be expressed as

$$\begin{aligned} e(k+1) &= v_d(k+1) - v(k+1) \\ &= v_d(k+1) - \Phi(k)v(k) - \Gamma\tau(k) - d(k) \end{aligned} \tag{59}$$

Substituting (55) into (59) and noting (54) gives

$$e(k+1) = C_1^{-1}[\sigma(k+1) - b(k+1)] \tag{60}$$

Substituting (50) into (60) yields

$$e(k+1) = C_1^{-1}\{\sigma(k+1) - \sigma(k) + C_1 e(k) - C_2\mathbf{g}[e(k)]\} \tag{61}$$

Since when $k > k_0$ there is $\sigma(k) = \mathbf{0}$, then (61) can be rewritten as

$$e(k+1) = e(k) - C_1^{-1}C_2\mathbf{g}[e(k)] \tag{62}$$

Consider the Lyapunov candidate as

$$V(k) = e_i^2(k), i = u, v, r \tag{63}$$

Now, the following two cases are considered:
*Case 1:* $|e_i(k)| > \alpha_1$. We have

$$e_i(k+1) = e_i(k) - \alpha_2 c_{1i}^{-1} c_{2i}\mathrm{sign}[e_i(k)] \tag{64}$$

Then the first-order difference of the Lyapunov function can be derived as

$$\begin{aligned} \Delta V(k) &= e_i^2(k+1) - e_i^2(k) \\ &= |\alpha_2 c_{1i}^{-1} c_{2i}|^2 - 2\alpha_2 c_{1i}^{-1} c_{2i}|e_i(k)| \\ &< (\alpha_2 c_{1i}^{-1} c_{2i} - 2\alpha_1)\alpha_2 c_{1i}^{-1} c_{2i} \end{aligned} \tag{65}$$

Since $\alpha_2 c_{1i}^{-1} c_{2i} - 2\alpha_1 < 0$, then $\Delta V(k) < 0$.
*Case 2:* $|e_i(k)| \le \alpha_1$. It obtains

$$e_i(k+1) = e_i(k) - \alpha_2 c_{1i}^{-1} c_{2i}\sin[\pi e_i(k)/2\alpha_1] \tag{66}$$

The first-order difference of (63) can be obtained as

$$\begin{aligned} \Delta V(k) &= e_i^2(k+1) - e_i^2(k) \\ &= (\alpha_2 c_{1i}^{-1} c_{2i})^2 \sin^2[\pi e_i(k)/(2\alpha_1)] - 2e_i(k)\alpha_2 c_{1i}^{-1} c_{2i}\sin[\pi e_i(k)/(2\alpha_1)] \\ &= \{\alpha_2 c_{1i}^{-1} c_{2i}\sin[\pi e_i(k)/(2\alpha_1)] - 2e_i(k)\}\alpha_2 c_{1i}^{-1} c_{2i}\sin[\pi e_i(k)/(2\alpha_1)] \end{aligned} \tag{67}$$

When $e_i(k) \ge 0$, the following deduction is obtained from (67)

$$\Delta V(k) \le [\alpha_2 c_{1i}^{-1} c_{2i}\pi/(2\alpha_1) - 2]\alpha_2 c_{1i}^{-1} c_{2i} e_i(k)\sin[\pi e_i(k)/(2\alpha_1)] \tag{68}$$

From the known conditions $0 \le e_i(k) \le \alpha_1$ and $\alpha_2 c_{1i}^{-1} c_{2i} < 4\alpha_1/\pi$, it can be deduced that $\Delta V(k) \leqslant 0$.

When $e_i(k) < 0$, we have $\alpha_2 c_{1i}^{-1} c_{2i}\sin[\pi e_i(k)/(2\alpha_1)] < 0$ and

$$\alpha_2 c_{1i}^{-1} c_{2i}\sin[\pi e_i(k)/(2\alpha_1)] - 2e_i(k) > [\alpha_2 c_{1i}^{-1} c_{2i}\pi/(2\alpha_1) - 2]e_i(k) \tag{69}$$

Since $\alpha_2 c_{1i}^{-1} c_{2i} < 4\alpha_1/\pi$, then according to (67), we know that $\Delta V(k) \leqslant 0$.

In summary, by reasonably selecting the values of $\alpha_1$ and $\alpha_2$ to satisfy $\alpha_2 c_{1i}^{-1} c_{2i} < 4\alpha_1/\pi$, the asymptotic convergence of the velocity tracking error $e_i(k)$ can be guaranteed, that is, the output $\nu(k)$ of the DSM closed-loop control system can stably track the reference input $\nu_d(k)$. From the conclusion of the virtual heading controller in Section 4.1, it can be known that the tracking error $\psi_e(k)$ of the DPS to the desired heading can asymptotically converge to zero. Furthermore, according to the conclusion of the guidance law design in Section 3.3, the position tracking error of the DPS can asymptotically converge to zero, i.e., $\Theta(k) \to 0$ , $k \to \infty$, which realizes the accurate following of the desired path.

## 6. Simulation

In this section, to verify the effectiveness and superiority of the proposed DPS path-following method based on the desired non-switching variable generator DSM control, the CyberShip II model established in Skjetne et al. (2004) is selected for comparative simulation analysis. The specific parameters of the ship model are as follows: $m = 23.8$ kg, $X_{\dot{u}} = -2.0$, $Y_{\dot{v}} = -10.0$, $N_{\dot{r}} = -1.0$, $Y_{\dot{r}} = 0$, $N_{\dot{v}} = 0$, $x_g = 0.046$, $X_u = -0.72253$, $Y_v = -0.88965$, $Y_r = -7.250$, $N_v = 0.0313$, $N_r = -1.900$, and its length is $L_{CS2} = 1.255$ m.

The initial position and heading angle of the DPS are set as: $x(0) = -10$ (m), $y(0) = 3$ (m), and $\psi(0) = -45°$. The initial velocities of the DPS are set as follows: $u(0) = 0$ (m/s), $v(0) = 0$ (m/s), $r(0) = 0$ (rad/s). The initial desired velocities of the DPS are set as follows: $u_d(0) = 0.25$ (m/s), $v_d(0) = 0.09$ (m/s), $r_d(0) = 0.2$ (rad/s). In order to create an environment in which the DPS operates under time-varying sideslip, set $v_d$ to a time-varying value. The desired surge and sway velocities of the DPS are set as: $u_d(t) = 0.25$ (m/s) and $v_d(t) = 0.09\sin(0.017t)$ (m/s). External environmental disturbances, including winds, waves and currents, are simulated as follows: $\omega_i = 10[\sin(0.5t)+\cos(0.5t+\pi/4)]+0.5, i = u, v, r$. The desired path of the DPS is set as: $x_p(\theta) = \theta$ (m), $y_p(\theta) = 10\sin(\theta/15)$ (m), where the path parameter $\theta$ is given by (26).

The relevant parameters of the guidance law design part of this paper are: $\varphi_1 = 0.1$, $\varphi_2 = 0.001$, $W = 1.69$, $\Delta_{\max} = 5.02$, $\Delta_{\min} = 4.3925$, $\kappa = 10$, and $k_x = 100$. The parameters of the high-order DDO are: $N = 2$, $L_0 = 0.1441$, $L_1 = 0.3960$, and $L_2 = 0.650$. The parameters of the DSM controller are: $h = 0.01$, $\xi = 1$, $\alpha_1 = 0.5$, $\alpha_2 = 1$, $\sigma_0 = [5, 5, 5]^T$, $C_1 = diag(0.75, 1, 100)$, and $C_2 = diag(0.2, 0.2, 0.01)$.

In order to better demonstrate the superiority of the proposed DSM path following control strategy, the comparative studies with DSM controller based on reference trajectory of switching variables (Bartoszewicz and Adamiak, 2020) and non-switching variable DSM controller (Bartoszewicz and Lesniewski, 2016) are performed.

The simulation results are shown in Figs. 4–16. Figs. 4 and 5 show the desired and actual path of the DPS with and without time-varying environmental disturbances and sideslip, respectively. In both cases, the proposed DSM control strategy realizes the fast and accurate following of the desired path by the DPS. Fig. 6 shows the variation of the

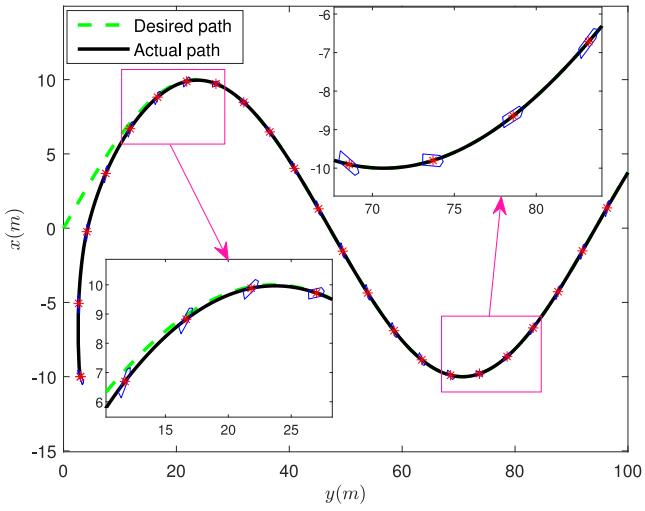


**Fig. 4.** The path of DPS with sideslip angle.

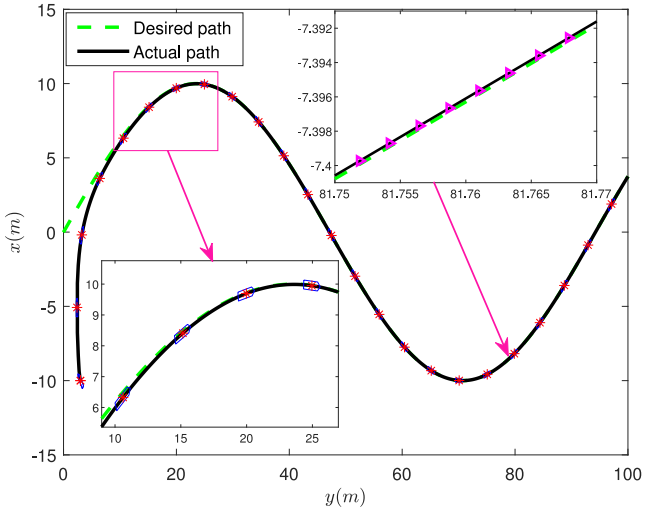


**Fig. 5.** The path of DPS without sideslip angle.

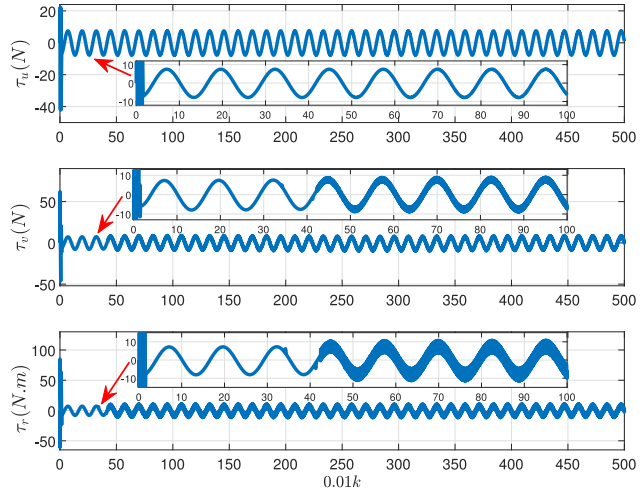


**Fig. 6.** The control inputs.

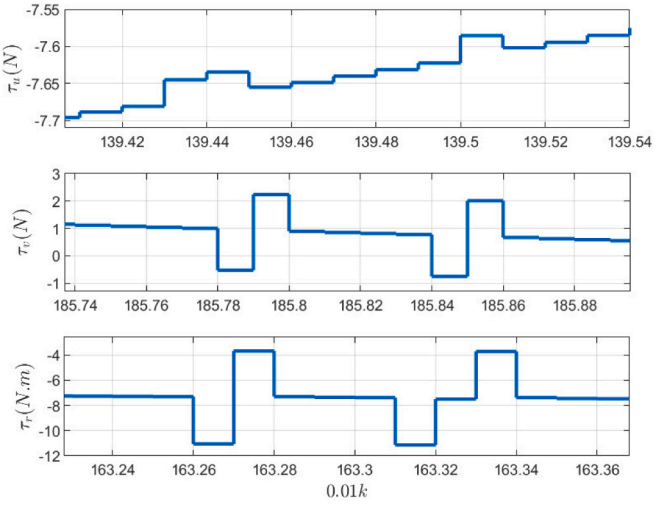


**Fig. 7.** The local magnification of control inputs.

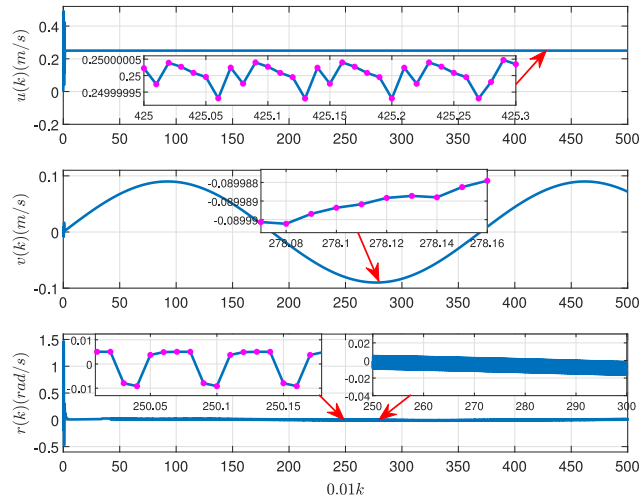


**Fig. 8.** The velocity change graph.

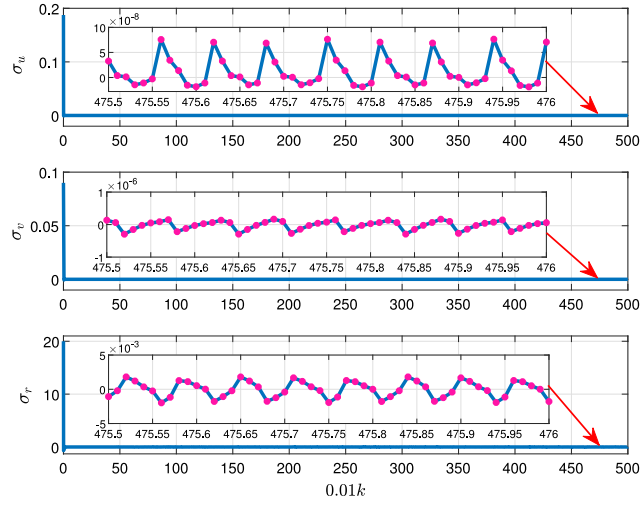


**Fig. 9.** The sliding variables (this paper).

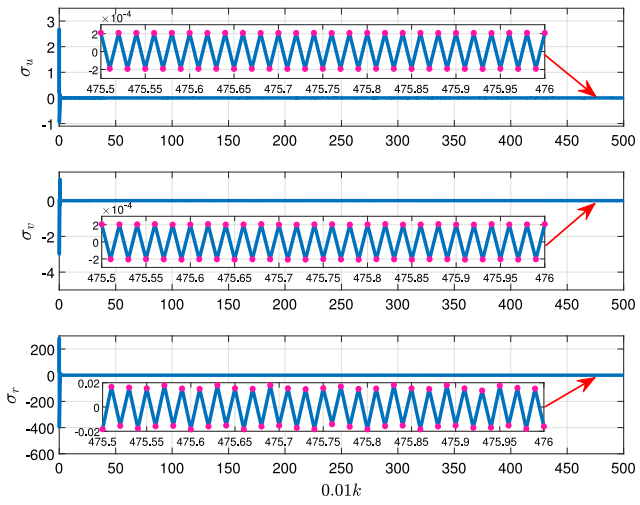


**Fig. 10.** The sliding variables (Bartoszewicz and Adamiak, 2020).

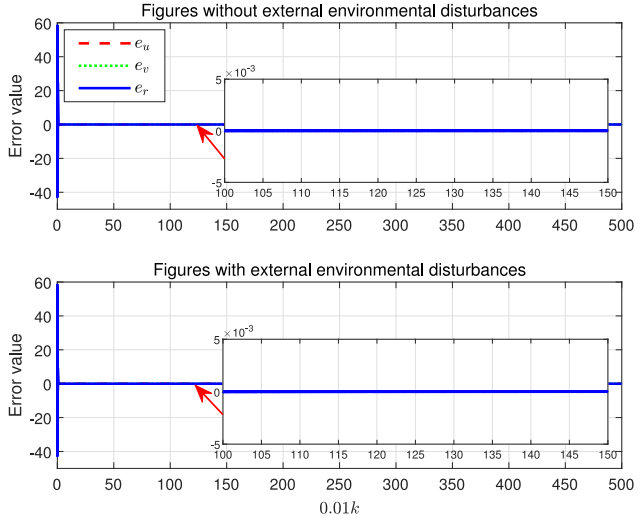


**Fig. 11.** The velocity tracking errors (this paper).

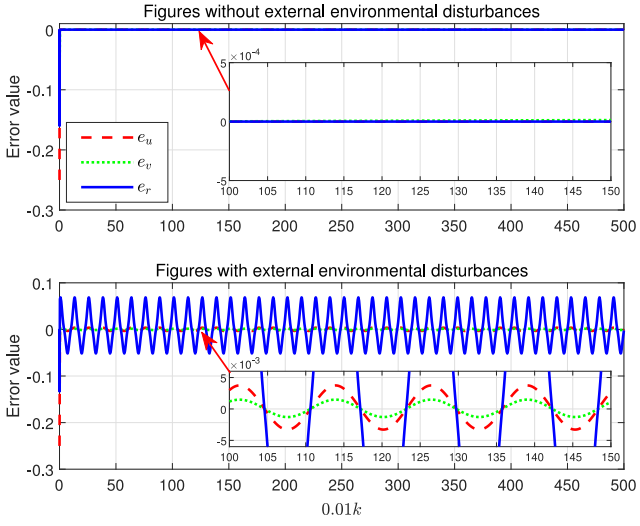


**Fig. 12.** The velocity tracking errors (Bartoszewicz and Lesniewski, 2016).

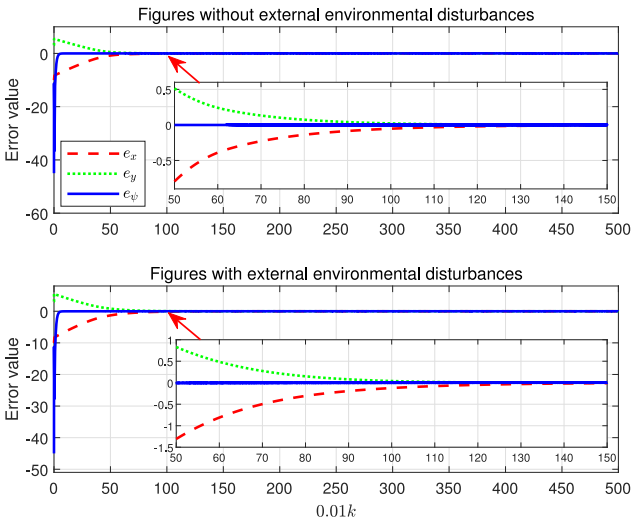


**Fig. 13.** The position tracking errors (this paper).

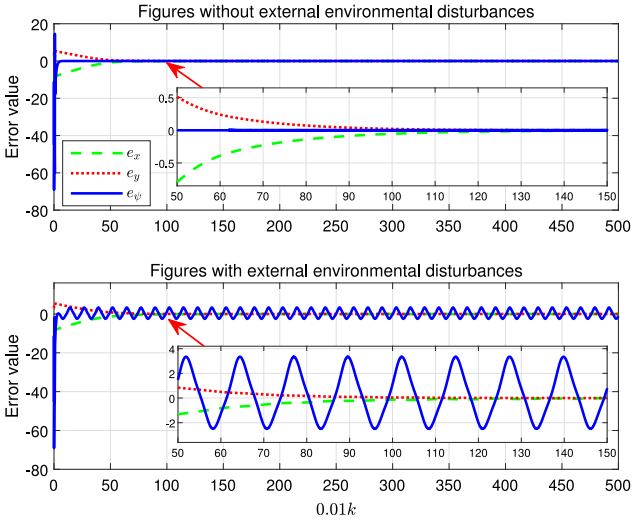


**Fig. 14.** The position tracking errors (Bartoszewicz and Lesniewski, 2016).

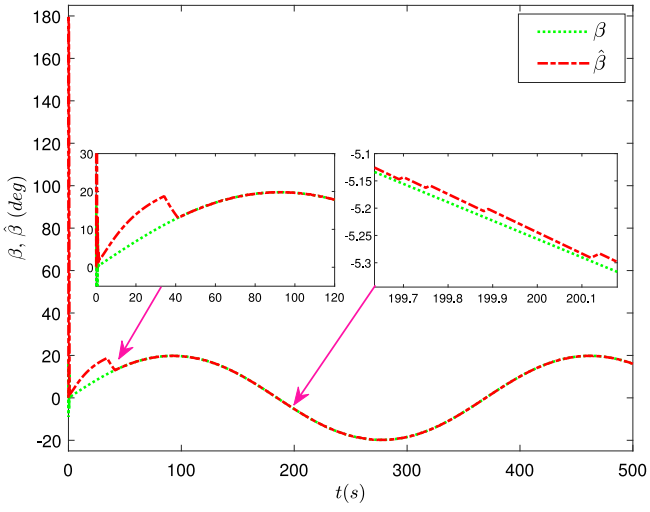


**Fig. 15.** The actual and observed sideslip angle.

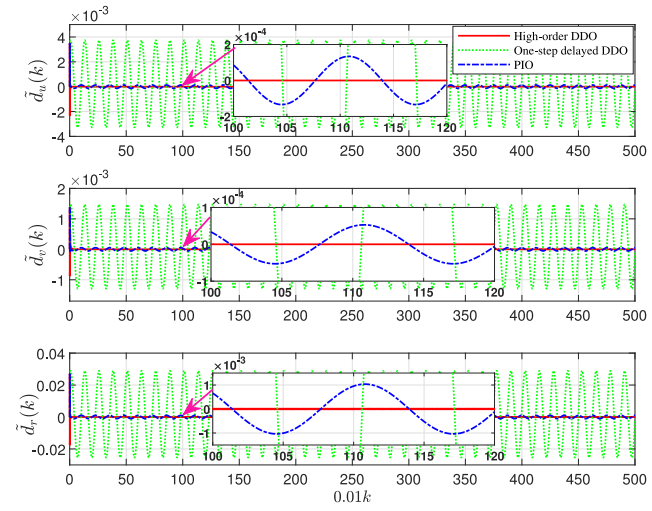


**Fig. 16.** Comparison of observation errors of three kinds of DDO.

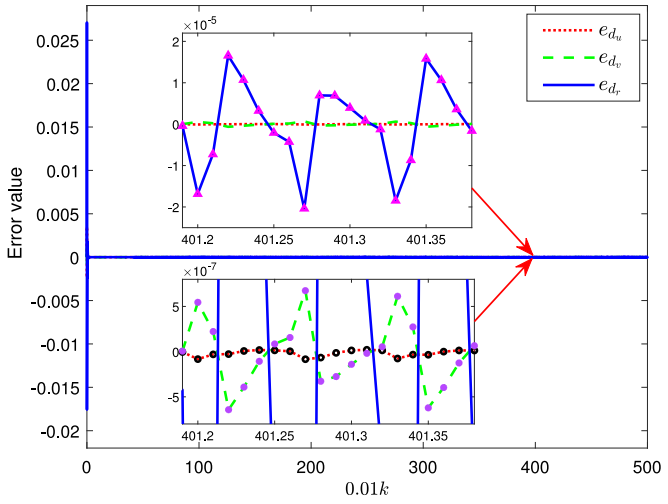


**Fig. 17.** The disturbance $d(k)$ observation errors.

control input. The bounds of the control input in the surge, sway and yaw degrees of freedom are ±42 N, ±62 N and ±85 N · m, respectively, and the bounds after stabilization are ±8 N, ±10 N and ±12 N · m, respectively. The small-amplitude chattering phenomenon after $k > 4000$ is caused by the observation error of the sideslip angle constantly fluctuating near zero due to the influence of sign function and signal preservation when the continuous-time sideslip angle observer is directly used in the discrete-time system, as shown in Fig. 15. When the sideslip angle is not considered, the control input chattering disappears. It also shows the necessity of designing discrete-time controllers for discrete-time systems in practical engineering.

Fig. 7 is a local magnification of the control input, showing the inherent control holding phenomenon within the sampling step of the discrete-time control input. The local irregular jump is the timely correction of the large deviation caused by the multiple holding of the control input by the discrete-time controller. Fig. 8 shows the velocity variation of the DPS. It can be seen that the surge and sway velocity curves of the DPS are smooth enough, while the yaw angular velocity curve has high-frequency vibration within ±0.01°, which can be considered smooth due to its tiny amplitude. Therefore, it can be seen that the proposed control strategy is effective in weakening DSM chattering.

To further verify the superiority of the designed DSM controller in anti-chattering, it is compared with a DSM controller (Bartoszewicz and Adamiak, 2020) based on switching variable reference trajectory. Figs. 9 and 10 show the variation of the sliding variables of the proposed controller and the controller based on the switching variable reference trajectory, respectively. In contrast, the sliding variables of the proposed controller has a smaller chattering amplitude, lower frequency, and smoother waveform.

In addition, to verify the anti-disturbance ability of the designed DSM controller, it is compared with a non-switching variable DSM controller (Bartoszewicz and Lesniewski, 2016). Figs. 11 and 12 show the velocity tracking errors of the proposed controller and the controller based on the reference trajectory of non-switching variables, respectively. The average absolute values of the velocity tracking errors $e_u$(m/s), $e_v$(m/s), and $e_r$(rad/s) of the two control strategies are $\{3.58\times10^{-8}, 1.26\times10^{-7}, 7.78\times10^{-6}\}$ and $\{9.43\times10^{-18}, 8.90\times10^{-6}, 5.48\times10^{-19}\}$, respectively, when there is no external environmental disturbance; and $\{3.58\times10^{-8}, 1.26\times10^{-7}, 9.91\times10^{-6}\}$ and $\{0.0022, 8.84\times10^{-4}, 0.0318\}$, respectively, when there is external environmental disturbance. In the case of external environmental disturbances, there is no chattering in the curve of the proposed controller, but obvious chattering occurs in the compared controller. Figs. 13 and 14 show the position tracking error diagrams of the proposed controller and the DSM controller based on the reference trajectory of switching variables, respectively. The mean absolute values of the position tracking errors $e_x(m)$, $e_y(m)$ and $e_\psi(deg)$ of the two control strategies are both 0.0011, 0.0025 and 0.0024 when there is no external environmental disturbance; and they are $\{0.0011, 0.0025, 0.0024\}$ and $\{0.026, 0.0125, 1.6711\}$ when there is the external environmental disturbance, respectively. Figs. 11–14 are the combination of error diagrams with and without external environmental disturbances. As can be seen from Figs. 11 and 13, there is almost no change in the tracking errors of the velocity and position of the controller proposed in this paper with and without external environmental disturbances. As can be seen from Fig. 12 and Fig. 14, the velocity and position tracking errors of the control system based on the control scheme of Bartoszewicz and Adamiak (2020) and Bartoszewicz and Lesniewski (2016) fluctuate obviously after adding external environmental disturbances. It can be seen that the proposed control scheme can greatly reduce chattering, and the anti-disturbance ability is also guaranteed.

Fig. 15 shows the variation of the actual sideslip angle and sideslip angle observation values of the DPS, which shows that the sideslip angle observer can track the actual sideslip angle within 40 s, and the tracking accuracy is high. Fig. 16 shows the observation errors of the high-order DDO in this paper, the one-step delay DDO in Xu (2016), and the PIO in Chang (2006). It can be seen that the observation effect of the high-order DDO is better. Fig. 17 shows the observation errors of disturbances. The designed high-order DDO can accurately observe external environmental disturbances within 80 s, and the observation error is less than one-thousandth of the actual value, which verifies the effectiveness of the high-order DDO. Therefore, the above comparative simulation results show that the proposed control scheme has higher efficiency and better control performance.

## 7. Conclusion

Aiming at the path following control problem of DPS under unknown environmental disturbances and sideslip, a DSM path following control scheme is designed. In order to weaken system chattering caused by switching functions and ensure the anti-disturbance advantage of the sliding mode control based on reference trajectory simultaneously, a new DSM reaching law based on non-switching reference trajectory is designed. A high-order DDO is designed to observe environmental disturbances and is used to design of the reaching law. A finite-time sideslip angle observer is designed to ensure the path following of the DPS under the time-varying sideslip. By replacing

the traditional integral with a nonlinear integral, a new discrete-time nonlinear integral SMS is designed, which not only avoids the possible integral saturation but also reduces the steady-state error and enhances the robustness. The comparative simulation results illustrate the effectiveness and performance of the proposed control scheme. The discrete-time design of the whole control process, including the discrete-time guidance law, will be considered in future research.

## CRediT authorship contribution statement

**Mingyu Fu:** Supervision, Software, Writing – original draft, Investigation. **Guorong Zhang:** Methodology, Software, Writing – original draft, Writing – review & editing. **Yujie Xu:** Validation, Software, Writing – original draft, Writing – review & editing.

## Declaration of competing interest

The authors declare that they have no known competing financial interests or personal relationships that could have appeared to influence the work reported in this paper.

## Data availability

Data will be made available on request.

## Acknowledgments

This work was supported by the National Natural Science Foundation of China under Grant 52071112.

## References

Abdelaal, M., Frazle, M., Hahn, A., 2018. Nonlinear model predictive control for trajectory tracking and collision avoidance of underactuated vessels with disturbances. Ocean Eng. 160, 168–180.
Adamiak, K., 2020. Reference sliding variable based chattering-free quasi-sliding mode control. IEEE Access 8, 133086–133094.
Bartoszewicz, A., 1998. Discrete-time quasi-sliding-mode control strategies. IEEE Trans. Ind. Electron. 45 (4), 633–637.
Bartoszewicz, A., Adamiak, K., 2020. Discrete-time sliding-mode control with a desired switching variable generator. IEEE Trans. Autom. Control 65 (4), 1807–1814.
Bartoszewicz, A., Lesniewski, P., 2016. New switching and nonswitching type reaching laws for SMC of discrete time systems. IEEE Trans. Control Syst. Technol. 24 (2), 670–677.
Bessa, W.M., Dutra, M.S., Kreuzer, E., 2010. An adaptive fuzzy sliding mode controller for remotely operated underwater vehicles. Robot. Auton. Syst. 58 (1), 16–26.
Chang, J.L., 2006. Applying discrete-time proportional integral observers for state and disturbance estimations. IEEE Trans. Autom. Control 51 (5), 814–818.
Fossen, T.I., 2011. Handbook of Marine Craft Hydrodynamics and Motion Control. Wiley.
Fu, Y., Li, B., 2022. Saturation constraint one-step optimal control of electrode current for the fused magnesia smelting process. Acta Autom. Sin. 48 (1), 239–248.
Fu, M., Wang, Y., Zhu, X., 2019. Modern Ship Dynamic Positioning. National Defense Industry Press.
Fu, M., Zhang, G., Xu, Y., 2022. Path tracking of dynamic positioning ship based on MIMO self-coupling PI controller. In: OCEANS 2022 - Chennai. pp. 1–6.
Gao, Z., Guo, G., 2020. Command filtered path tracking control of saturated ASVs based on time varying disturbance observer. Asian J. Control 22 (3), 1197–1210.
Gao, W., Wang, Y., Homaifa, A., 1995. Discrete-time variable structure control systems. IEEE Trans. Ind. Electron. 42 (2), 117–122.
Gonzalez-Garcia, A., Castaeda, H., 2021. Adaptive integral terminal sliding mode control for an unmanned surface vehicle against external disturbances. IFAC Papersonline 54 (16), 202–207.
Hu, Z., Hu, W., Wang, Z., 2018. A sliding mode control with nonlinear integrator for matrix rectifier. Power Electron. 52 (3), 3.
Hu, Y., Wang, H., He, S., Zheng, J., Ping, Z., Shao, K., Cao, Z., Man, Z., 2021. Adaptive tracking control of an electronic throttle valve based on recursive terminal sliding mode. IEEE Trans. Veh. Technol. 70 (1), 251–262.
Islam, M., Mills, J., Gash, R., Pearson, W., 2021. A literature survey of broken ice-structure interaction modelling methods for ships and offshore platforms. Ocean Eng. 221.
Jung, C.Y., Yoo, S.L., 2019. Optimal rescue ship locations using image processing and clustering. Symmetry 11 (1).
Kang, S., Wu, H., Yang, X., Li, Y., Lu, H., 2021. Discrete-time predictive sliding mode control for a constrained parallel micropositioning piezostage. IEEE Trans. Syst. Man Cybern. A 1–12.
Li, Y., An, L., Jiang, Y., He, J., Cao, J., Guo, H., 2018b. Dynamic positioning test for removable of ocean observation platform. Ocean Eng. 153, 112–121.
Li, X., Sun, G., Shao, X., 2020. Discrete-time pure-tension sliding mode predictive control for the deployment of space tethered satellite with input saturation. Acta Astronaut. 170, 521–529.
Li, T., Zhao, R., Chen, C., Fang, L., Liu, C., 2018a. Finite-time formation control of under-actuated ships using nonlinear sliding mode control. IEEE Trans. Cybern. 48 (11), 3243–3253.
Liu, C., Li, Y., Tian, S., Ma, H., 2021. Disturbance compensation based discrete-time sliding mode control with a reference trajectory generator. Int. J. Control Autom. Syst. 19 (12), 3862–3868.
Liu, L., Wang, D., Peng, Z., 2017. ESO-based line-of-sight guidance law for path following of underactuated marine surface vehicles with exact sideslip compensation. IEEE J. Ocean. Eng. 42 (2), 477–487.
Ma, H., Xiong, Z., Li, Y., Liu, Z., 2021. Design of discrete-time sliding mode control with disturbance compensator based switching function. IEEE Trans. Circuits Syst. II 68 (4), 1268–1272.
Mathiyalagan, K., Sangeetha, G., 2020. Second-order sliding mode control for nonlinear fractional-order systems. Appl. Math. Comput. 383.
Peng, Z., Wang, J., 2018. Output-feedback path-following control of autonomous underwater vehicles based on an extended state observer and projection neural networks. IEEE Trans. Syst. Man Cybern. A 48 (4), 535–544.
Peng, L.I., Zheng, Z.Q., 2011. Sliding mode control approach with nonlinear integrator. Control Theory Appl. 28 (5), 619–624.
Piorno, J.R., Roman, S.S., Giron-Sierra, J.M., De, L., 2009. Fast ship electronic system for seakeeping experimental studies. IEEE Trans. Instrum. Meas. 58 (10), 3427–3433.
Qu, Y., Cai, L., Xu, H., 2021. Curved path following for unmanned surface vehicles with heading amendment. IEEE Trans. Syst. Man Cybern. A 51 (7), 4183–4192.
Rubagotti, M., Incremona, G.P., Raimondo, D.M., Ferrara, A., 2021. Constrained nonlinear discrete-time sliding mode control based on a receding horizon approach. IEEE Trans. Autom. Control 66 (8), 3802–3809.
Sanjeewa, S., Parnichkun, M., 2021. Control of rotary double inverted pendulum system using LQR sliding surface based sliding mode controller. J. Control Decis. 9 (1), 89–101.
Shao, X., 2015. Research on Control Methods for Dynamic Positioning Ships Based on Discrete System Theory (Master's thesis). Harbin Engineering University.
Shao, K., Xu, F., Zheng, J., Wang, X., 2021. Nested adaptive integral terminal sliding mode control for high-order uncertain nonlinear systems. Int. J. Robust Nonlinear Control 31 (14), 6668–6680.
Sharma, N.K., Roy, S., Janardhanan, S., 2021. New design methodology for adaptive switching gain based discrete-time sliding mode control. Int. J. Control 94 (4), 1081–1088.
Sheng, Y., Jiang, W., Pei, P., Zhou, Y., 2020. Discrete-time angle constraint interception with model-assisted target maneuver estimator. Int. J. Aerosp. Eng. 2020 (60), 1–12.
Shtessel, Y., Shkolnikov, I., Levant, A., 2007. Smooth second-order sliding modes: Missile guidance application. Automatica 43 (8), 1470–1476.
Skjetne, R., Smogeli, O.N., Fossen, T.I., 2004. A Nonlinear Ship Manoeuvering Model: Identification and adaptive control with experiments for a model ship. Model. Identif. Control 25 (1), 3–27.
Sørensen, A., 2011. A survey of dynamic positioning control systems. Ann. Rev. Control 35 (1), 123–136.
Van, M., Mavrovouniotis, M., Ge, S.S., 2019. An adaptive backstepping nonsingular fast terminal sliding mode control for robust fault tolerant control of robot manipulators. IEEE Trans. Syst. Man Cybern. A 49 (7), 1448–1458.
Wang, Y., 2019. Research on Active Disturbance Rejection Control Method of USV Path Following (Master's thesis). Harbin Engineering University.
Wang, N., Ki Ahn, C., 2020. Hyperbolic-tangent los guidance-based finite-time path following of underactuated marine vehicles. IEEE Trans. Ind. Electron. 67 (10), 8566–8575.
Wu, W., Peng, Z., Wang, D., Liu, L., Gu, N., 2022. Anti-disturbance leader–follower synchronization control of marine vessels for underway replenishment based on robust exact differentiators. Ocean Eng. 248, 110686.
Xu, Q., 2016. Digital integral terminal sliding mode predictive control of piezoelectric-driven motion system. IEEE Trans. Ind. Electron. 63 (6), 3976–3984.
Zhang, G., Zhang, X., 2014. Concise robust adaptive path-following control of underactuated ships using dsc and mlp. IEEE J. Ocean. Eng. 39 (4), 685–694.